

Inelastic Analysis of Power Plant Components under Transient Thermal Environment

K. Naumenko^{1a}, A. Kutschke^{1b}, Y. Kostenko^{2a} and Th. Rudolf^{2b}

¹Martin-Luther-University Halle-Wittenberg, Center of Engineering Sciences, 06099 Halle, Germany, ^{1a}konstantin.naumenko@iw.uni-halle.de, ^{1b}andreas.kutschke@iw.uni-halle.de,

²Siemens AG, Energy Sector, Rheinstr. 100, Mülheim an der Ruhr, 45478 Germany,

^{2a}yevgen.kostenko@siemens.com, ^{2b}thorsten.rudolf@siemens.com

ABSTRACT. *We utilize phenomenological constitutive equations that describe inelastic behavior of advanced 9-12%Cr heat-resistant steels at high temperature and multi-axial stress state. The model is calibrated against experimental creep curves and verified for different isothermal and non-isothermal loading paths. We analyze an idealized start-up, holding and shut-down sequence of a component under a moderate temperature gradient. To estimate the thermal fields, transient heat transfer analysis is performed. The results are applied in the subsequent structural analysis using the developed inelastic constitutive model. The outcome is a multi-axial thermo-mechanical fatigue loop which can be used for a damage assessment.*

INTRODUCTION

Many important components of steam turbines operate under severe temperature environment and mechanical loadings over a long period. Critical positions like notches or welds may be subject to fatigue damage due to thermal transients and/or creep damage during holdings at high temperature. Generally, the structural integrity of a component is ensured through reliable design, precise manufacturing, definition of allowable operational modes, and timely inspection. However, permanently changing economic situations and environmental conditions require more flexible operation modes in service, e.g. daily start-up and shut-down and/or increase of steam pressure and temperature. The demand for higher flexibility and efficiency could be reached by reliable life-time assessments through the use of adequate structural analysis and material testing.

The aim of this paper is to analyze a power plant component during an idealized start-up, holding and shut-down sequence under a moderate temperature gradient. In particular, we generate a multi-axial thermo-mechanical fatigue (TMF) loading loop as a result of non-stationary thermal environment. Towards this goal, we utilize a robust constitutive model that reflects inelastic deformation processes in advanced 9-12%Cr heat resistant steels under service-type loading conditions at high temperature. To characterize hardening, recovery and softening processes we apply a multi-axial model of binary mixture with inelastic-hard and inelastic-soft constituents. Creep damage processes are characterized by a state variable in the sense of continuum damage mechanics. The material constants

and the response functions in the model are calibrated against experimental creep curves under tensile and compressive loading. For the verification, simulations of the inelastic response under different loading paths are performed and the results are compared with experimental data.

For a steam temperature profile corresponding to a typical hot start-up, transient heat transfer analysis of an idealized steam turbine rotor is performed to compute the temperature field. The results are applied for the subsequent mechanical analysis using the developed inelastic constitutive model. To illustrate the local loading changes over the whole cycle, appropriate values of stresses and strains are presented. The results build a base for creep and fatigue damage assessment.

CONSTITUTIVE MODEL

Below we address the modeling of inelastic processes in advanced 9-12%Cr heat resistant steels designed for the use at steam temperatures up to 650°C. We limit the range of temperatures to 350 – 650°C. To explain the model assumptions, let us begin with the uni-axial stress state.

A materials science approach to the modeling of inelastic behavior is based on the composite having inelastic-hard and inelastic-soft constituents [1]. The corresponding inelastic strain rates are characterized by independent, physically motivated laws, where densities of mobile dislocations and their mean velocities are considered. The inelastic-hard constituent is associated with subgrain boundaries. The corresponding volume fraction is related to microstructural parameters such as the mean subgrain size. Because both the subgrain and the carbide microstructures tend to coarsen, the volume fraction is assumed to decrease towards a certain saturation value. The advantage of this approach is the possibility of simulation hardening as a result of stress redistribution between the constituents and softening due to the decrease in volume fraction. However, this approach is currently limited to the uni-axial stress state.

A similar approach in continuum mechanics is based on a mixture model with two or more constituents with different inelastic properties. The basic assumption is that the internal force is non-uniformly distributed over an infinitesimal area element as a result of inelastic deformation. To approximate this distribution, two or more stress tensors can be introduced. With the balance equations and constitutive assumptions for the partial stresses, the constitutive model for the inelastic mixture can be formulated. The material parameters and response functions are identified from the macroscopic data on tensile and/or creep behavior.

Let us introduce an iso-strain mixture with two constituents. To designate the properties of the constituents we use the subscripts s (inelastic-soft) and h (inelastic-hard), respectively. Let ε_s and ε_h be the strains of the constituents and σ_s and σ_h the corresponding effective stresses. With the iso-strain approach we can write

$$\sigma = (1 - \eta_h)\sigma_s + \eta_h\sigma_h, \quad \dot{\varepsilon} = \dot{\varepsilon}_h = \dot{\varepsilon}_s, \quad (1)$$

where η_h is the volume fraction of the inelastic-hard constituent. We assume that the behavior of the constituents is governed by the following equations

$$\dot{\epsilon}_s = \frac{d}{dt} \left(\frac{\sigma}{9K} + \frac{\sigma_s}{3G} \right) + f(|\sigma_s|)g(T) \frac{\sigma_s}{|\sigma_s|}, \quad \dot{\epsilon}_h = \frac{d}{dt} \left(\frac{\sigma}{9K} + \frac{\sigma_h}{3G} \right) + \frac{\sigma_h - \sigma}{\sigma_{h*} - \sigma} |\dot{\epsilon}^c|, \quad (2)$$

where K is the bulk modulus, G is the shear modulus, $\sigma_{h*}(\sigma)$ is the saturation stress value in the hard constituent and ϵ^c is the average inelastic strain of the mixture. $f(x)$ is a monotonically increasing function with $f(0) = 0$ and $g(T)$ is the Arrhenius type function of the absolute temperature T . With the new variables

$$\beta = \frac{\sigma_h - \sigma}{c_h}, \quad \beta_* = \frac{\sigma_{h*} - \sigma}{c_h}, \quad \Gamma = \frac{c_h \eta_h}{1 - \eta_h}, \quad \Gamma_* = \frac{c_h \eta_{h*}}{1 - \eta_{h*}}, \quad c_h = \frac{1 - \eta_{h0}}{\eta_{h0}},$$

where η_{h0} is the reference value of η_h , Eqs (1) and (2) can be transformed to

$$\dot{\epsilon}^c = f(|\sigma - \beta\Gamma|)g(T) \frac{\sigma - \beta\Gamma}{|\sigma - \beta\Gamma|} - \frac{d}{dt} \left(\frac{\beta\Gamma}{3G} \right), \quad \dot{\beta} = \frac{1}{G} \frac{dG}{dT} \dot{T} \beta + \frac{3G}{c_h} \left(\dot{\epsilon}^c - |\dot{\epsilon}^c| \frac{\beta}{\beta_*} \right) \quad (3)$$

In Eqs (3) β , $0 \leq \beta \leq \beta_*$ and Γ , $\Gamma_* \leq \Gamma \leq 1$ play the role of internal state variables. The underlined term has a minor influence on the inelastic strain rate and can usually be neglected [2]. If the fraction is kept constant then by setting $\Gamma = 1$ we obtain the kinematic hardening/recovery model proposed in [3]. Therefore, the variable $\beta\Gamma$ can be termed backstress or kinematic stress. Let us assume that Γ decreases with the increase of the average inelastic strain towards the saturation value $\Gamma_*(\sigma)$ viz

$$\dot{\Gamma} = A_s(\Gamma_* - \Gamma)|\dot{\epsilon}^c|, \quad (4)$$

where A_s is a constant. Then the set of Eqs (3) and (4) describes the decrease of the strain rate as a result of stress redistribution between the constituents and the increase of the strain rate as a consequence of softening processes.

Figure 1 shows the experimental data for 12%Cr steel after [4]. Creep tests were performed under constant compressive and tensile true stress levels. The creep rate vs. creep strain curves under compression clearly show the hardening and softening regimes. Based on the experimental data, the material constants and response functions in Eqs (3) and (4) are identified. Tensile creep curves under the same stress levels exhibit higher tertiary creep rate, Fig. 1. The results of metallographic analysis show that tertiary creep under tension is additionally controlled by the nucleation and growth of voids [4]. To consider creep damage we introduce the parameter ω in the sense of continuum damage mechanics [5]. The constitutive and the damage evolution equation are postulated as follows

$$\dot{\epsilon}^c = f \left(\frac{|\sigma - \beta\Gamma|}{1 - \omega} \right) g(T) \frac{\sigma - \beta\Gamma}{|\sigma - \beta\Gamma|}, \quad \dot{\omega} = r(\omega)h(\sigma) \frac{|\dot{\epsilon}^c|}{\epsilon_*(\sigma)}, \quad (5)$$

where $r(\omega)$, $h(\sigma)$ and $\epsilon_*(\sigma)$ are response functions. Based on tensile creep curves, Eqs (5) are calibrated. The results are presented in Fig. 1 by lines. The material constants and

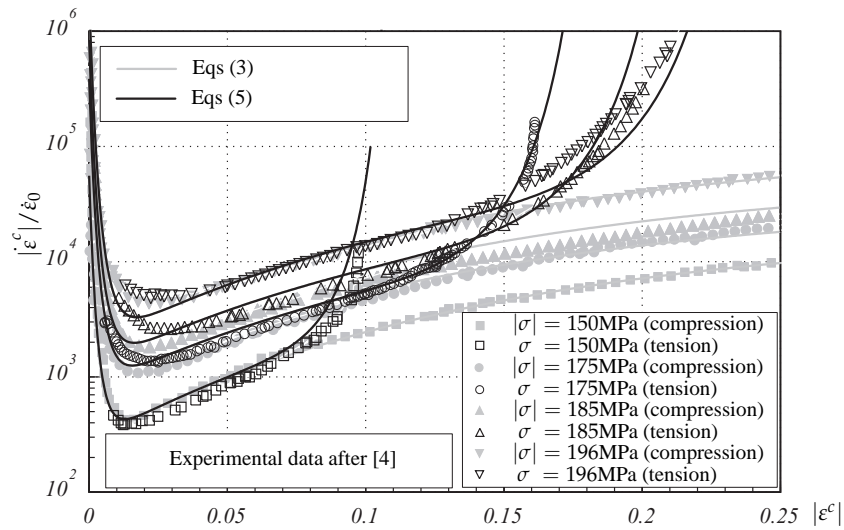


Figure 1. Normalized creep rate vs. creep strain for X20CrMoV12-1 steel at 600°C

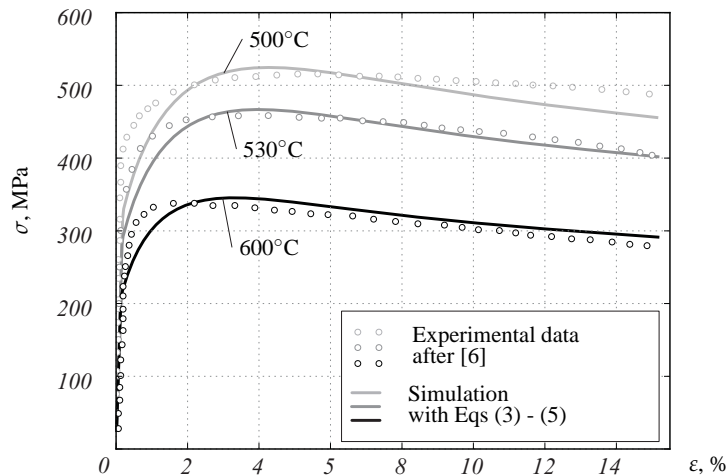


Figure 2. Stress-strain diagrams for X20CrMoV12-1 steel at $\dot{\epsilon} = 2.63 \cdot 10^{-4} \text{ s}^{-1}$

response functions were determined for a class of 9-12%Cr steels. For X20CrMoV12-1 steel the values are presented in [2].

For the verification of the model we performed simulations of inelastic responses under different loading paths. Figure 2 shows the experimental stress-strain diagrams obtained in [6]. The solid line presents the model prediction. Although the transition from the linear-elastic to the viscoplastic behavior is too strict, the maximum stress values and the softening behavior are well reproduced by the model. Figure 3 illustrates the simulation results of the stress response under TMF loading. Experimental data for such strain and temperature controls are presented in [7] for uni-axial specimens from 10%Cr steel

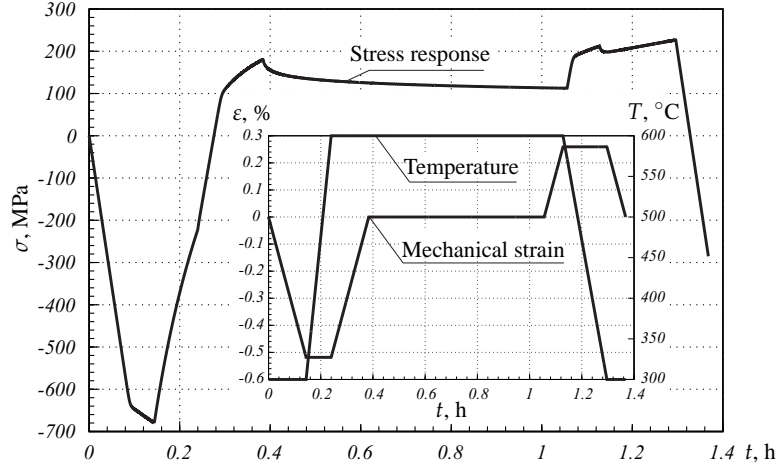


Figure 3. Stress response under TMF loading path for X20CrMoV12-1 steel

and in [8] for cruciform specimens from 1%Cr steel under biaxial loading. Although for X20CrMoV12-1 steel such data are not available, the results presented in Fig. 3 qualitatively meet experimental data published in [7]. In [2] several examples are presented that verify the model for different isothermal, stress-controlled tests. It is shown, that the model reproduces experimental creep curves after rapid loading changes. Furthermore, it provides a good estimation of long-term strength curves in a wide stress range.

To generalize the model to multi-axial stress states we assumed small (elastic and inelastic) strains. Let $\boldsymbol{\varepsilon}$ be the infinitesimal strain tensor, $\boldsymbol{\varepsilon}^c$ the corresponding inelastic part and $\boldsymbol{\sigma}$ the Cauchy stress tensor. Equations (3) - (5) are generalized as follows [2]

$$\begin{aligned}
 \dot{\boldsymbol{\varepsilon}}^c &= \frac{3}{2} f \left(\frac{\bar{\sigma}_{vM}}{1 - \omega} \right) g(T) \frac{\bar{\mathbf{s}}}{\bar{\sigma}_{vM}}, \quad \bar{\mathbf{s}} = \mathbf{s} - \Gamma \boldsymbol{\beta}, \quad \mathbf{s} = \boldsymbol{\sigma} - \frac{1}{3} \text{tr} \boldsymbol{\sigma} \mathbf{I}, \quad \bar{\sigma}_{vM} = \sqrt{\frac{3}{2} \text{tr} (\bar{\mathbf{s}})^2}, \\
 \dot{\boldsymbol{\beta}} &= \frac{1}{G} \frac{dG}{dt} \dot{\boldsymbol{\beta}} + \frac{2G}{c_h} \left(\dot{\boldsymbol{\varepsilon}}^c - \frac{3}{2} \dot{\varepsilon}_{vM} \frac{\boldsymbol{\beta}}{\beta_*(\sigma_{vM})} \right), \quad \dot{\varepsilon}_{vM} = \sqrt{\frac{2}{3} \text{tr} (\dot{\boldsymbol{\varepsilon}}^c)^2}, \\
 \dot{\Gamma} &= A_s [\Gamma_*(\sigma_{vM}) - \Gamma] \dot{\varepsilon}_{vM}, \quad \sigma_{vM} = \sqrt{\frac{3}{2} \text{tr} (\mathbf{s})^2}, \\
 \dot{\omega} &= r(\omega) h(\boldsymbol{\sigma}) \frac{\dot{\varepsilon}_{vM}^c}{\varepsilon_{*}(\sigma_{vM})}, \quad h(\boldsymbol{\sigma}) = \frac{1}{2} \frac{(\sigma_I + |\sigma_I|)}{\sigma_{vM}},
 \end{aligned} \tag{6}$$

where \mathbf{s} is the stress deviator, \mathbf{I} is the second rank unit tensor, $\boldsymbol{\beta}$ is the kinematic stress deviator and σ_I is the maximum principal stress.

HEAT TRANSFER AND STRUCTURAL ANALYSIS

As an example, let us consider an idealized steam turbine rotor. Figure 4 shows a sketch

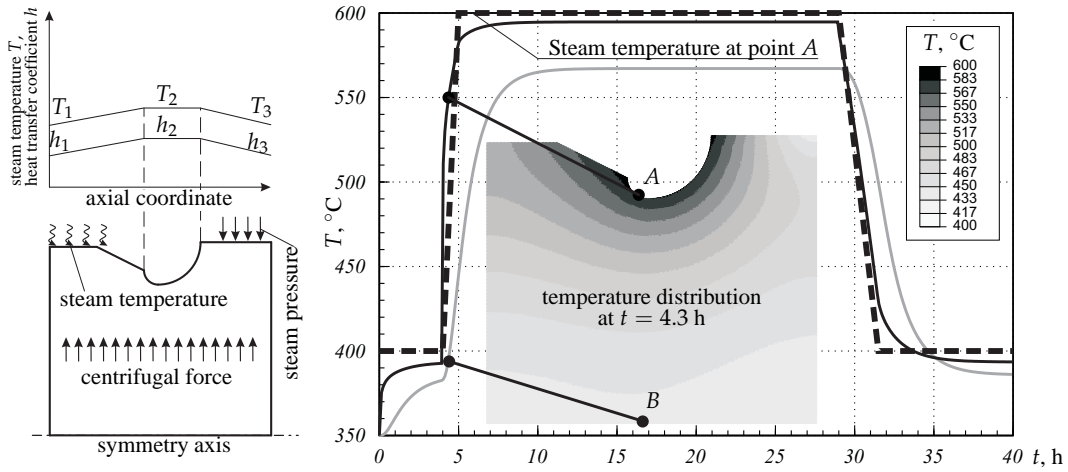


Figure 4. Geometry, loading and temperature profile in a rotor

of geometry, loading and temperature distributions. The material properties are specified for X22CrMoV12-1 steel. The steam temperature profile on the surface of the rotor corresponds to an idealized hot start. The maximum steam temperature T_2 in the notched area is increased from 400°C up to 600°C , kept 600°C and decreased down to 400°C , Fig. 4. The changes in the steam density and velocity during warm-up and cool-down are taken into account by the time varying heat transfer coefficients h_i . To compute the temperature field in the component, transient heat transfer analysis is performed by the finite element program ABAQUS. The time variation of the temperature in two selected points A and B are shown in Fig. 4. At $t = 4.3$ h during warm-up the greatest difference between the temperatures at A and B is observed. The contour plot illustrates the corresponding temperature distribution.

The obtained temperature field as well as primary loads (steam pressure on the surface of the rotor and the centrifugal force) are applied for the subsequent structural analysis. The constitutive model (6) is utilized inside ABAQUS by a user material subroutine. Figure 5a illustrates time variations of the mechanical strain tensor $\tilde{\boldsymbol{\varepsilon}} = \boldsymbol{\varepsilon} - \alpha_T \Delta T \mathbf{I}$ in the point A of the surface, where α_T is the coefficient of thermal expansion. The corresponding time variation of the stress state is presented in Fig. 5b. Due to the confidentiality of material parameters the results for the absolute values of strains and stresses were normalized. Therefore, they should be considered in a just qualitative manner. Let us note that the normal \mathbf{n} , the tangential \mathbf{t} and the circumferential \mathbf{e}_φ directions on the surface are the principal directions of both the stress and the strain tensors. The strain component $\tilde{\varepsilon}_{nn}$ is determined by the Hookes law as $\tilde{\varepsilon}_{nn} = \text{tr } \boldsymbol{\sigma} / 3K - (\tilde{\varepsilon}_{tt} + \tilde{\varepsilon}_{\varphi\varphi})$ while $\sigma_{nn} = -p$, where p is the steam pressure. Based on time variations of $\tilde{\varepsilon}_{tt}$, $\tilde{\varepsilon}_{\varphi\varphi}$, σ_{tt} and $\sigma_{\varphi\varphi}$ one may recognize the local compression during heat-up with the maximum at $t = 4.3$ h, the creep range characterized by an increase in strain and the stress relaxation during the holding and the local tensile regime during shut-down with the peak at $t = 32.5$ h. From Fig. 6a

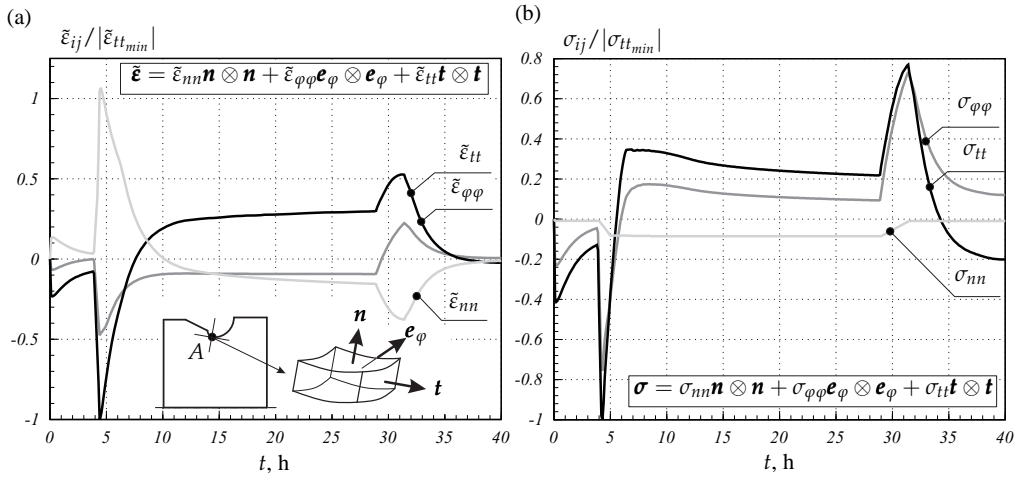


Figure 5. Local loading vs. time at Point A: (a) mechanical strain tensor; (b) stress tensor

we observe that the local loading is non-proportional. Note that only the principal values of the strain tensor are non-proportionally changing while the principal directions are approximately fixed. The local hysteresis loops presented in Fig. 6b are consistent with the experimental data under idealized uni-axial and bi-axial loading conditions [7, 8].

CONCLUSIONS AND RECOMMENDATIONS

The aim of this paper was to analyze inelastic behavior in a power plant component under

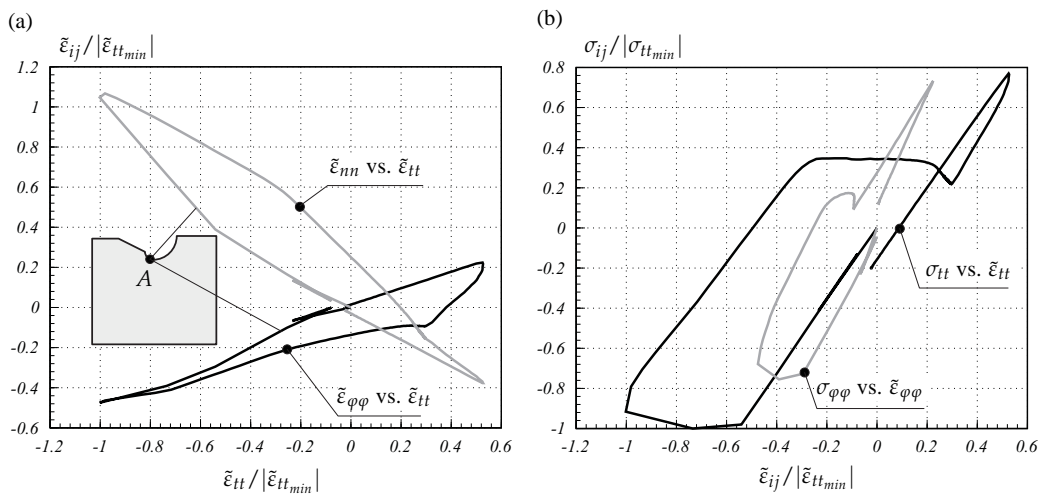


Figure 6. Local loading paths at point A: (a) strain paths; (b) hysteresis loops

realistic non-isothermal loading. The principal outcome is the possibility to generate the multi-axial TMF loading loops over one or several cycles. Based on the results we may conclude as follows

- The obtained hysteresis loops are qualitatively consistent with the test results for cruciform and notched specimens under TMF loading [7, 8]. Structural analysis over several loading cycles and experimental data provide an input for the fatigue life estimations.
- The stress and strain states during holdings correspond to the typical creep regime. Estimation of creep damage and creep life in a structure under stationary loading and temperature is provided by the constitutive model like (6). Examples for creep damage analysis in structures are presented in [5, 9], among others.
- Although constitutive models like (6) are able to reflect local deformation behavior and creep damage, surface induced fatigue damage processes, e.g. formation of micro-extrusions are currently not accounted for. Based on generated multi-axial TMF loops and related material testing, further investigations to elaborate driving force(s) and kinetics for fatigue damage should be performed.

REFERENCES

- [1] Blum, W. (2008) In: F. Abe, T.U. Kern and R. Viswanathan (Eds.), *Creep-Resistant Steels*, pages 365 – 402. Woodhead Publishing, Cambridge.
- [2] Naumenko, K., Altenbach, H. and Kutschke, A. (2010) *Int. J. Damage Mech.* In press.
- [3] Frederick, C.O. and Armstrong, P.J. (2007) *Mater. High Temp.* **24**(1), 1 – 26.
- [4] Straub, S. (1995) Dissertation, Universität Erlangen-Nürnberg, Fortschr.-Ber. VDI Reihe 5, Nr. 405, Düsseldorf.
- [5] Naumenko, K. and Altenbach, H. (2007) *Modelling of Creep for Structural Analysis*. Springer, Berlin et al.
- [6] Röttger, D. (1997) Dissertation, Universität GH Essen, Fortschr.-Ber. VDI Reihe 5, Nr. 507, Düsseldorf.
- [7] Cui, L., Scholz, A., von Hartrott, P. and Schlesinger, M. (2009) Abschlussbericht, AVIF Vorhaben Nr. 895, FVV, Heft 888, Frankfurt am Main.
- [8] Samir, A., Simon, A., Scholz, A. and Berger, C. (2006) *Int. J. Fatigue* **28**(5-6), 643 – 651.
- [9] Kostenko, Y., Schwass, G. and Naumenko, K. (2009) In: I.A. Shibli and S.R. Holdsworth (Eds.), *Creep & Fracture in High Temperature Components*, pages 797 – 805. DEStech Publications, Lancaster, Pennsylvania.